Journal of Information Technology Management

Print ISSN: 2008-5893

Online ISSN: 2423-5059

Early Diagnosis of Alzheimer Disease from Mri Using Deep Learning Models

Apparna Allada*

*Corresponding Author, Research Scholar, Department of CSE Annamalai University, Chidambaram, Email: alladaaparna9@gmail.com

R. Bhavani

Prof., Department of CSE, Annamalai University, Chidambaram, Email: bhavaniaucse@gmail.com

Kavitha Chaduvula

Professor, Department of IT SR Gudlavalleru Engineering College, Gudlavalleru, Email: kavithachaduvula12@gmail.com

R. Priya

Professor, Department of CSE, Annamalai University, Chidambaram, Email: prykndn@yahoo.com

Abstract

On a global scale, one of the prevalent causes of dementia is Alzheimer's disease (AD). It will cause a steady deterioration in the individual from the mild stage to the severe stage, and thus impair their capacity to finish any tasks with no aid. The diagnosis is done with the utilization of existing methods which include medical history; neuropsychological testing as well as MRI (Magnetic Resonance Imaging), a lack of sensitivity as well as precision does affect the consistency of efficient procedures. With the deep learning network's utilization, it is possible to create a framework for detecting specific AD characteristics from the MRI images. While automatic diagnosis is done with the application of diverse machine learning techniques, the existing ones do suffer from certain constraints with regards to accuracy.

Thus, this work's key goal is to increase the classification's accuracy through the inclusion of a pre-processing approach prior to the deep learning model. The Alzheimer's disease Neuroimaging Initiative (ADNI) database of AD patients was used to develop a deep learning approach for AD identification. In addition, this study will present ideas for Haralick features, feature extraction from Local Binary Pattern (LBP), Artificial Neural Network (ANN), and Visual Geometry Group (VGG)-19 network techniques. The results of the experiments show that the deep learners offered are more effective than other systems already in use.

Keywords: Alzheimer's disease (AD), Magnetic Resonance Imaging (MRI), Deep Learning (DL), Artificial Neural Network (ANN) and Visual Geometry Group (VGG).

Journal of Information Technology Management, 2023, Vol. 15, Special Issue, pp. 52-71
Published by University of Tehran, Faculty of Management
doi: https://doi.org/10.22059/jitm.2022.89411
Article Type: Research Paper

Received: February 26, 2022
Received in revised form: May 07, 2022
Accepted: August 18, 2022
Published online: October 19, 2022

Introduction

Adolescents and those over the age of @65 are more likely to be diagnosed with Alzheimer's disease (AD) than those under that age group. This disease's characterization will involve a progressive cognitive decline that is inclusive of decline in memory, cognitive and attention. At present, AD does not have any curative treatments. However, with various promising pharmacologic compounds in the advanced developmental stages, there is anticipation that there will be a breakthrough in treatment in the near future (Lu D et al., 2018). As of now, one of the factors behind the slow development of disease modifying treatments has been attributed to the incapacity in identifying patients in the stage of mild Cognitive impairment (MCI) which develops into AD. The failure of a potential promising AD treatment can occur when its administration does not seem to be beneficial to individuals with MCI symptoms (Taheri Gorji H & Kaabouch N, 2019).

Early interventions during in the AD's course may aid in delaying the onset and/or mitigating the risk of confrontation of full-blown AD. Treatments during a later stage of the AD's may slow down the disease's progression but reversal of the already-occurred pathology-induced neuronal loss cannot be treated (Altinkaya E et al., 2020). This is yet another reason as to why it is essential to recognize individuals with prodromal AD at the MCI stage. Therefore, the diagnosing of the MCI stage in AD is a critical task, as well as urgent upon the availability of curative treatments. In addition, such diagnoses can be important for individuals with MCI due to reasons excluding AD, since the identification as well as the management of these other reasons may be much simpler and easier (Raghunath, K. M. Karthick et al., 2021).

The ADNI has recently specified new criteria for the categorization of MCI patients into two separate groups: the Early MCI (EMCI) and the Late MCI (LMCI) (ADNI). Discrimination between the two separate groups will be based on the degree of memory impairment (Saba S S et al., 2020) When compared to the normative mean, the memory loss in EMCI patient's ranges from 01.0–01.5 SD; in contrast, in LMCI patients, the memory loss is at least 01.5 SD more than the normative mean. Research on ageing is difficult because it must distinguish between two separate groups of patients, i.e., between those who have EMCI

and those who have normal ageing, due to the similarity in brain structure between those with normal ageing and those with MCI (Kang S K et al., 2021)

Diagnostic methods such as MRI, functional magnetic resonance imaging (fMRI), computed tomography (CT), single-photon emission computed tomography (SPECT), and positron emission tomography (PET) is the most commonly used by medical researchers and doctors in the diagnosis of MCI and AD (PET). MRI is a medical imaging technology that uses computer-assisted devices to produce pictures of the body's various areas while using radio waves. Detection and diagnosis are the most common uses of this approach. Protons in water, which are the building blocks of biological tissues, are used to create a movement shift in the axis of this technology. Two strong circular magnets will be used in an MRI machine (Kumar S S & Nandhini M, 2021). A major part of the human body is composed of water molecules with oxygen as well as hydrogen atoms. At each atom’s center, there are protons which will act as magnets, and also are sensitive to the magnetic field. When a radiofrequency current is applied on the patient, these protons will undergo stimulation, and thus, will end up spinning the numerous protons of the body. Upon closure of the radiofrequency field, there will be exposure of the signal detected by the MRI scanner’s receiver part. Methods of biomedical imaging biomedical imaging will process these signals to generate an MR image (Saikumar K & Rajesh V, 2020).

During the imaging procedure, the patient has to keep still for a long time so as not to blur the MR image. This in turn, will bring along certain problems. For faster acquirement of the image, an intravenous method is employed on the patient, either prior to the MRI or during the procedure, in order to boost the image quality as well as the speed of acquisition (Muthukumaran V et al., 2021). Nowadays, enhancement of the image acquisition’s quality as well as speed is done through utilization of numerous biomedical imaging methods.

Extraction of features from the image will constitute the next step of automatic diagnosis. wherein the features will get extracted from diverse textures so that there is maximization of the within-class similarity as well as minimization of the between-class similarity (Liu S et al., 2021). The feature extraction’s objective is to extract data from images which can be used by the machine learning algorithms. The Local Binary Pattern (LBP) has been presented in this work as a fast, simple as well as extremely effective method for the extraction of features from the image texture. Initially, there is selection of an image’s neighbourhood in this method. Later, there is comparison of the intensity of this neighbourhood’s existing points with that of the neighbourhood’s centrally-situated pixel, and also each pixel will be considered as a binary code. A circular neighbourhood is typically taken into account so as to make the algorithm rotation-invariant (Mahesh, T. R et al., 2022).

DL is a category of AI in which a network will classify generally from the given dataset, that may be sound, text, or pictures. In general, the neural network architecture will actualize the deep learning. The network will become deeper with the increase in the number of layers.

When compared with The Conventional Neural Networks (CNNs) having two or three layers, the DNN's can have multiple layers. Deep learners have delivered results which are equivalent to, and even at certain times, better than that of the human experts (Dhiman, G et al., 2021).

In recent times, proposals for various deep learning-based approaches for resolving diverse problems of computer vision have demonstrated results that were far better than that of the traditional algorithms (Mohammed B A et al., 2021). Primarily, this is because improvements in the computational power will enable the handling of huge datasets based on the highly manipulated neural network structures, and thus, will allow them to resolve the complex problems. When compared with the standard mathematical as well as statistical approached, one among the deep learning's numerous benefits is the relative simplicity in configuring the relationship between the input space as well as the output space in diverse situations (Toğaçar M et al., 2021). Hence, these approaches have been rapidly deployed in the field of medical imaging, and also have accomplished incredible successes in image classification, segmentation, noise reduction as well as image generation. In this work, a framework for AD detection based on Harlick and LBP feature extraction, ANN classifier and VGG-19 network is presented (Ljubic B et al., 2020).

Literature Review

Presently, structural brain Magnetic Resonance Images (sMRI) data is widely used for evaluating the brain anatomical changes, and has resulted in early AD detection by means of deep networks. However, the chief issues which affect the existing AD models are the unreliability as well as complex pre-processing. In order to overcome these issues, Kumar & Nandhini had proposed a feature extraction model (FEESCTL) with entropy slicing as well as Transfer Learning for the purpose of classification. During the training process, the suggested framework used the entropy image slicing approach to identify the most informative MRI slices. The VGG-16 network used Transfer Learning to train on the ADNI dataset in order to better classify people with Alzheimer's disease than had previously been possible using just data from the general population. A 93% accuracy in binary classifications (AD/MCI; MCI/CN; AD/CN) and a 93.22% accuracy in ternary classifications (AD/MCI/CN) could be deduced from the results of the experiments, which showed that the suggested model had achieved these levels of accuracy (Lei B et al., 2022). Moreover, comparative analysis was used for confirmation of the model's efficiency in diagnosing AD (Praveen Sundar, P.V et al., 2021).

Pan offered the proposal for a CNN-based ensemble model of multi-slice classifiers for the early diagnosis of AD as well as for the identification of the significant brain regions which were associated with the AD. Genome-Wide Association Studies (GWAS) was performed for further investigation into the AD's potential genetic biomarkers through

utilization of the identified brain regions' morphological data as well as the genotype (Ahmed S et al., 2019).

(Kouser, R.R et al., 2018) had put forward a DL- based model for AD detection from the ADNI database of AD patients, a dataset that was composed of fMRI as well as PET images of AD patients as well as of normal individuals. The authors had employed 3D to 2D conversion as well as image resizing prior to the application of the CNN's VGG-16 architecture for the extraction of features. In the end, the classification was done with the use of K means clustering, SVM, Linear Discriminate, Decision tree classifiers (Bevilacqua V et al., 2017). The simulation outcomes had showed that the fMRI dataset's classification had accomplished 99.95% average accuracy whilst the PET dataset's classification had accomplished 73.46% average accuracy. Upon comparison of these outcomes in terms of accuracy, specificity, sensitivity as well as on a few other parameters, it was found that these outcomes were much superior to those of the existing approaches (Kale V V et al., 2019).

Liu et al had constructed a reference model which was based on the volumes as well as thicknesses of earlier-reported regions of the brain which were associated with the disease progression. The proposed deep-learning model was found to be more accurate as well as substantially quicker than the volume/thickness model. In addition, the network was found to be applicable for forecast progression: subjects with MCI who had been misclassified by the model as being mild AD dementia patients had quicker progressions to dementia over time. The proposed model's analysis of the learned features had showed its reliance on an extensive range of regions which were associated with AD. It was evident from these findings that the DNN were capable of automatically learning how to identify imaging biomarkers where were predictive of AD, and thus, leverage them to accomplish accurate as well as early AD detection (Aguilar C et al., 2013).

This proposed method was composed of the following two DL- based models: I) Image segmentation and II) Classification of image. At first, a model, that had combined the Gaussian Mixture Model (GMM) as well as the CNN, was used for segmentation of the brain tissues. Later, these segmented tissues were employed for AD classification by means of a new model that was a combination of the Extreme Gradient Boosting (XGBoost) as well as the Support Vector Machine (SVM). Two evaluations were submitted by the authors for segmentation and classification. The proposed method's comparative analysis was done via utilization of the AD-86 dataset, and the AD-126 dataset (V., Muthukumaran et al., 2021). The results had demonstrated that both datasets had obtained Dice 00.96 for segmentation, and accuracies of 00.88, and 00.80 respectively, for classification.

In order to extract multilevel discriminative MRI characteristics for the diagnosis of dementia, (Kumar V V et al., 2021) suggested an attention-guided DL architecture. At initially, the authors had designed a backbone fully convolutional network for the automatic localization of the discriminative regions of the brain. ADNI-1, ADNI-2, and AIBL datasets

were used for evaluating the proposed method. The proposed method had displayed superior performance when compared against various other advanced methods for tasks of MCI conversion prediction and AD diagnosis.

For the diagnosis of dementia, Mohammed et al proposed two CNN models (AlexNet and ResNet-50) as well as DL hybrid strategies (AlexNet+SVM and ResNet-50+SVM). It's worth noting that all models achieved good performance; however, the hybrid approaches (which combined DL and ML) outperformed the DL models. The AlexNet+SVM hybrid model has achieved 94.82 percent accuracy, 93.00 percent sensitivity, 97.85 percent specificity, and 99.75 percent AUC.

Toğaçar et al had submitted a dataset which was made up of MR images with the AD's four distinct phases. Re-enhancement of the dataset was done separately with the techniques of Deep Dream, fuzzy color image enhancement, and hyper column. There was utilization of the Visual Geometry Group-16 (VGG-16) deep learners in the enhancement method, and also there was combination of the deep features. The effective features were chosen via linear regression. The preferred classifier was the SVM. The proposed approach had accomplished an 99.94% overall accuracy with the classification results as 100% in Mild Dementia, 99.95% in Moderate Dementia, 100% in non-Dementia, and 99.95% in Very Mild Dementia. Through re-enhancement of MR images, the proposed method had improved the prediction success in the recognition of AD stages. As a result, there was realization of an efficient as well as affordable early diagnosis model which could be employed on individuals at most risk for progression of dementia.

Ljubic et al had made the determination that the diagnosis of AD from EMR data alone (with no reliance on investigative imaging) could be greatly enhanced through the application of clinical domain knowledge in data pre-processing as well as positive dataset selection instead of on setting naïve filters. The pool of heterogeneous ambulatory EMR data collected from primary care physician offices was mined for the information used in this study. The construction of a positive dataset from AD-relevant data was performed via application of medical domain knowledge. Selected Clinically Relevant Positive (SCRP) datasets were used as inputs to an LSTM Recurrent Neural Network (RNN) DL model to predict if a patient will acquire Alzheimer's disease (AD). Even so, when compared with the use of naïve dataset selection, the proposed model's performance was substantially better.

Lei et al had designed a joint DL achitectures for the prediction of AD's clinical scores. In particular, there was usage of feature assortment combining group LASSO and Correntropy for dimensionality reduction as well as for screening the features of the brain's AD-related regions. Multi-layer independently RNN regression was investigated by the authors as a means of examining the intrinsic connections between various brain areas and the temporal correlation between longitudinal data. In the proposed integrated DLN, MRI and clinical scores were evaluated and the clinical score predicted. The predicted values of the clinical

score had enabled the doctors to carry put early diagnosis as well as prompt treatment of the patients' disease condition.

Methodology

In this work, a five-class classification of AD is presented. The overall flow of investigation is shown in figure 1. In this section, the Haralick features, LBP, ANN and VGG-19 methods are discussed.

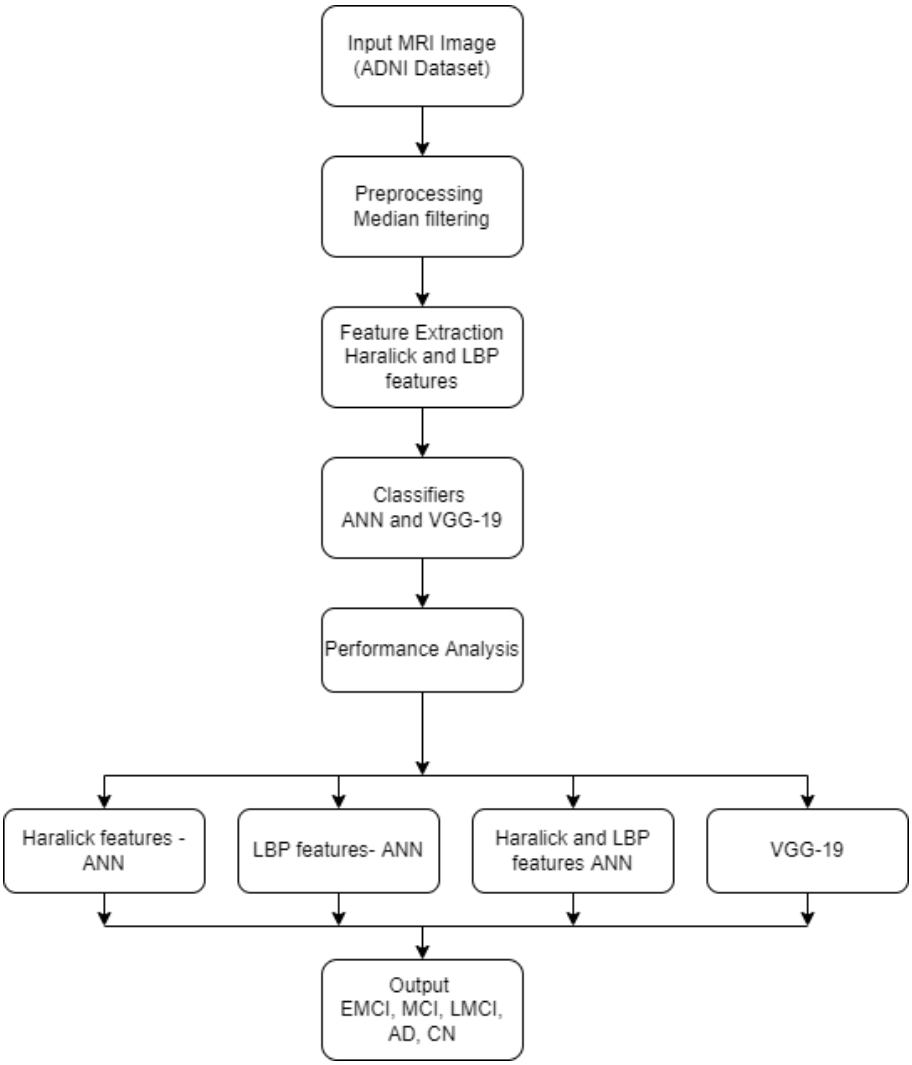

Figure 1. Overall Flow of Investigation

1. Dataset

This work's data has been taken from the ADNI, a global research effort which offers an active support for the investigation, analysis as well as improvement in AD treatments in order to mitigate its progression. Using the ADNI datasets, researchers will have access to a variety of datasets that may be used in different ways to help in the early diagnosis of AD.

Since it uses pre-existing data sets, ADNI paves the way for scholars all around the world to collaborate on research projects.

There were five categories of mild cognitive impairment (EMCI, LMCI), mild cognitive impairment (MCI), Alzheimer's disease (AD), and normal control subjects (CN) studied in this study. The ADNI databases provided all of the photos. The number of photos utilised for assessment is shown in Table 1.

Table 1. Datasets

Stage	No. of samples
Mild Cognitive Impairment (MCI)	263
Late MCI (LMCI)	72
Early MCI (EMCI)	240
Cognitive Normal (CN)	580
Alzheimer's disease (AD)	171
Total	1326

The following are the sample input Brain images for each stage depicted in figure 2:

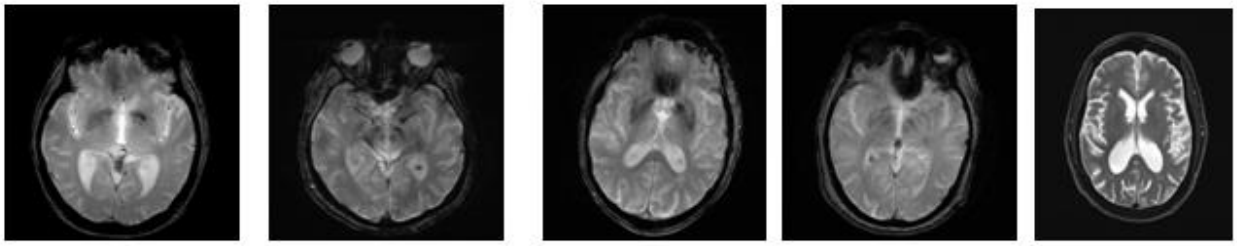

Figure 2. Sample input images. (a) MCI (b) LMCI (c) EMCI (d) CN (e) AD

2. Pre-processing

The task of pre-processing involves reading the data, de-noising the data and morphing the data. It is not confined to the above said operations. The raw data consists of various noises which may occur due to the capturing devices, light conditions. This data is to be transformed into a form that is required for processing. Pre-processing effectiveness and classification accuracy are inversely proportional. To reduce the amount of noise in a picture, a variety of filtering methods are used.

Median filters are used to minimise the amount of noise in photographs in this study. For example, a pixel's value may be changed by taking the median of the grey levels around it and applying it to the pixel's value. The original value of each pixel is taken into account when determining the median. Median filters with less blurring than similar-sized linear smoothing filters are more effective in reducing noise.

3. Haralick Features

Quantification of the texture content is a significant method to region description. The statistical moments from an image's or region's intensity histogram are used to describe textures. However, if just histograms are used to analyse texture, the information about the location of the pixels relative to each other is lost. This is a significant aspect of the texture description process, and one way to incorporate thus, texture-analysis must take into account an image's intensity distribution as well as the pixels relative positions.

Suppose that in an image f, there are L levels of potential intensity and that Q (d,) is an operator that specifies the location of two pixels separated by d in the direction. A matrix with an entry gij equal to the number of times the pixel pairings with intensities zi and zij will appear in the f at the position provided by Q is shown. The gray-level (or intensity) co-occurrence matrix is the name given to this matrix.

In the context of texture feature extraction and description, the grey co-occurrence matrix is susceptible to noise and picture rotation. To overcome this, we may use a set of position operators that sweeps across 180 degrees at the same distance parameter, D, to create a co-occurrence matrix. If D equals 1, there is a definite set of directions: 0, 45, 90, and 135 degrees (please refer Figure 3). Symmetric or asymmetric, the co-occurrence matrix may take into consideration both of these factors (which will take into account the gij as well as the gji elements).

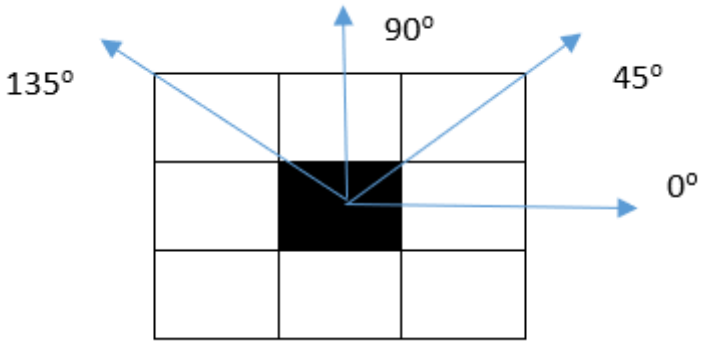

Figure 3. Representation of Instructions for obtaining the co-occurrence matrix.

Generally in an image, the number of potential image intensity level will determine the size of matrix G. G will have a size of 256 × 256 for an 8-bit image (i.e., 256 potential levels). While this is not an issue when working with a single matrix, at times, there is utilization of co-occurrence matrices in sequences. For the computational load's minimization load, an oft-employed method is to consider few bands for quantizing the intensities so as to maintain a manageable dimension of the matrix G.

n pixel pairings satisfying Q equals the sum of G's elements. Later, the number will estimate the chance that Q-satisfying points have values (zi, zj). The aggregate of these probability will be 1 according to Eq. (1):

$$\sum_{i=1}^{K}\sum_{j=1}^{K} p_{ij} = 1 \tag{1}$$

Here, K will denote the row (or column) dimension of square matrix G.

Below is the list of a set of descriptors that are useful for characterization of the at ease of G:

Correlation: This measures how linked a pixel is to its neighbour throughout the whole picture (Eq. (2) to Eq. 1 to 1 corresponds to perfect positive and negative correlations. However, if standard deviation is zero, this measure is not defined.

$$\sum_{i=1}^{K}\sum_{j=1}^{K} \frac{(i-m_r)(i-m_c)}{\sigma_r \sigma_c} \tag{2}$$

$$m_r = \sum_{i=1}^{K} i \sum_{j=1}^{K} p_{ij} \tag{3}$$

$$m_c = \sum_{j=1}^{K} j \sum_{i=1}^{K} p_{ij} \tag{4}$$

$$\sigma_r^2 = \sum_{i=1}^{K} (i-m_r)^2 \sum_{j=1}^{K} p_{ij} \tag{5}$$

$$\sigma_c^2 = \sum_{j=1}^{K} (\mathrm{j}-m_c)^2 \sum_{i=1}^{K} p_{ij} \tag{6}$$

Contrast: It measures the contrast between a pixel and its neighbour over the whole picture (see Eq. (7)). 0 (where G is constant) to (K 1)23

$$\sum_{i=1}^{K}\sum_{j=1}^{K} (i-j)^2 p_{ij} \tag{7}$$

Energy: It measures pixel intensity uniformity over the whole picture (see Eq. (8)). The values will be in the [0, 1] range. For a constant intensity image, the uniformity will be equivalent to 1.

$$\sum_{i=1}^{K} p_{ij}^2 \tag{8}$$

Homogeneity: Please refer to Eq. (9) for an example of how near the distribution of items in G is to the diagonal. When G is a diagonal matrix, the values will be in the [0, 1] range, with the maximum being achieved.

$$\sum_{i=1}^{K}\sum_{j=1}^{K}\frac{p_{ij}}{1+|i-j|} \tag{9}$$

Entropy: Eq. (10) provides an equation for determining how random the components of G are. When all pij are equal to 0, the entropy will be zero, and when all pij are equal, the entropy will be maximum. The highest possible value is 2 log2K.

$$-\sum_{i=1}^{K}\sum_{j=1}^{K} p_{ij}\log_2 p_{ij} \tag{10}$$

Inertia or Dissimilarity: It calculates the quantity of dissimilarity of the co-occurrence pairs. It gives the measure of difference in signal intensities.

$$\sum_{i=1}^{K}\sum_{j=1}^{K}|i-j|p_{ij} \tag{11}$$

Inverse Difference Moment: It computes the texture homogeneity.

$$\sum_{i=1}^{K}\sum_{j=1}^{K}\frac{p_{ij}}{1+|i-j|} \tag{12}$$

Cluster Prominence: It measures local intensity variation.

$$\sum_{i=1}^{K}\sum_{j=1}^{K}(1+j-2\mu)^3 p_{ij} \tag{13}$$

Haralick 13 texture features are extracted. The eight Haralick features are Correlation, contrast, energy, homogeneity, entropy, inertia; inverse difference moment and Cluster Prominence are used. Haralick features represent the texture quite accurately.

4. Local Binary Pattern (LBP)

In 1996, Ojala et al. had put forward the LBP as a local texture descriptor which today has turned into a well-known as well as effective feature descriptor in numerous applications because of its computational simplicity, robustness to monotonic gray-scale changes as well as ability to differentiate potential. The LBP [20] descriptor is able to evaluate each pixel's binary code. With the help of Eq. (14) and Eq. (15), we can evaluate the central pixel's LBP code inside the 3 × 3 neighborhood of each pixel as below

$$LBP_{P,R}=\sum_{p=0}^{p-1}\left(s\left(g_p-g_c\right)\right)^{2^p} \tag{14}$$

$$s(x)=0, \text{for } x<0;$$
$$1, \text{for } x>=0; \tag{15}$$

In the above equations, (P, R) will denote a neighborhood of P, while in the uniformly-placed sample points on a R-radius circle will have s (x) as the thresholding function, gcas the center pixel ingp, and p = 0, 1, . . . , P−1 denoting the pixels within the neighborhood.

5. ANN

An ANN's belong to a family of powerful algorithms. Since it draws inspiration from the nervous system, the ANN will model itself on how the brain will adapt on its own and learn. For an artificial neuron to operate, it has to include the following components: synapses, an adder (the cell membrane), and an activation function that determines whether or not to fire the input signals (threshold). When linear inputs are combined to produce non-linear functions, a neural network [21] yields an enormous number of different models, making it a very general statistical model. In addition, the model may accurately estimate any arbitrarily continuous function in Equation. (16)

$$y(in)_k = w_{0k} + \sum_i x_i w_{ik} \tag{16}$$

Where, xi = input of neuron i at input layer, Eq. (17) give the output:

$$y_k = f(y(in)_k) \tag{17}$$

Each output unit y_k(k = 1 to m)whose target is t_k, the error correction is computed by Eq. (18)

$$\delta_k = (t_k - y_k) f'(y(in)_k) \tag{18}$$

The weights are updated using Eq. (19)

$$\Delta\omega_{ik} = \alpha\delta_k n_j$$

$$\Delta\omega_{0k} = \alpha\delta_k \tag{19}$$

Where, wij = weight on ith neuron at hidden layer j, α = learning rate, δ_k is transferred to all the hidden layers, w0j = bias on jth hidden unit,ti = target output vector (t1, …, tk, …, tm), and nij = neuron i in jth hidden layer. The bias and weights of each output unit is updated using equation (20):

$$\omega_{jk}(new) = \omega_{jk}(old) + \Delta\omega_{jk}$$
$$\omega_{0k}(new) = \omega_{0k}(old) + \Delta\omega_{0k} \tag{20}$$

The sigmoid activation function as in Eq. (21):

$$g(x) = \frac{1}{1+e^{-x}} \tag{21}$$

Iteration of the aforementioned steps will occur either for specific epochs or till the actual output becomes equivalent to the target output. The learning rate, α , has a crucial role in the

network convergence wherein a higher value will result in speeding up the convergence but also will lead to overshooting, and vice versa. Therefore, a huge learning rate will cause rapid learning with oscillation of weights while a smaller learning rate will result in leisurely-paced learning. For a small learning rate α, the gradient descent will be slow, and it will widely vary for a huge α. The momentum factor's inclusion is done to mitigate the oscillation. $\eta \in [0,1]$ will represent the momentum factor while its will be set as 0.9. Here, the formulae for updating the weights will be as per Eq. (22) and Eq. (23):

$$\omega_{jk}(t+1) = \omega_{jk}(t) + \underbrace{\alpha\delta_k z_j + \eta\left[\omega_{jk}(t) - \omega_{jk}(t-1)\right]}_{\Delta\omega_{jk}(t+1)} \tag{22}$$

and

$$w_{ij}(t+1) = w_{ij}(t) + \underbrace{\alpha\delta_j x_i + \eta\left[w_{ij}(t) - w_{ij}(t-1)\right]}_{\Delta w_{ij}(t+1)} \tag{23}$$

Momentum factor helps faster convergence.

6. VGG-19 Networks

VGG CNN will constitute six major structures, wherein each structure is primarily made up of multiple connected convolutional layers as well as full-connected layers. While 3*3 is the convolutional kernel's size, 224*224*3 is the input size. 16~19 is the typical concentration of the number of layers. Figure 4 will provide an illustration of the VGG-19 model structure.

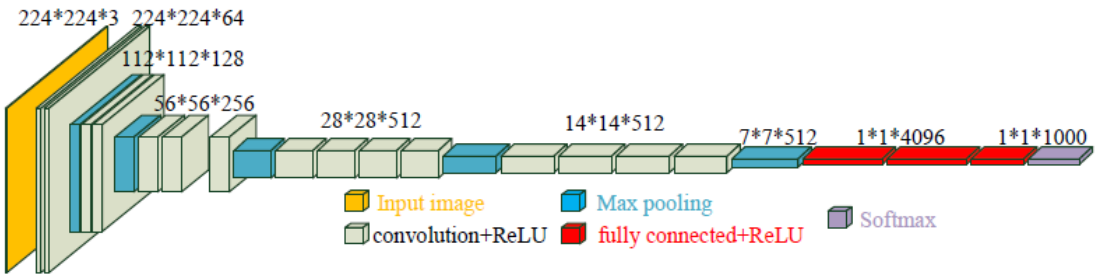

Figure 4.VGG-19 Network model

When compared against the conventional CNNs, this model has more enhancements in network depth. In lieu of a single convolution layer, it will utilize a better-performing interchanging structure of multiple convolutional layers as well as non-linear activation layers. The layer structure will have the following abilities: better image feature extraction, usage of max pooling for downsampling, and also modification of the linear unit (ReLU) as the activation function, in other words, choose the image area's biggest value as the area's pooled value. The downsampling layer is chiefly employed to enhance the network's anti-distortion capability to the image whilst retaining the sample's major features, and mitigating the number of parameters. Eq. (24) will provide the downsampling layer's expression.

Amongst them, down $\left(\chi_j^{(n-1)}\right)$ will denote the maximum pooling sampling function, τ_j^n will denote the coefficient which corresponds to the nth layer's jth feature map, and $f\left(\tau_j^n down\left(\chi_j^{(n-1)}\right)+b_j^{(n)}\right)$ will denote the ReLU activation function in Eq. (24).

$$\chi_{p_j}^{(n)} = f\left(\tau_j^n down\left(\chi_j^{(n-1)}\right) + b_j^{(n)}\right) \quad (24)$$

ReLU isa popularly used activation function due to its simplicity and effectiveness. The use of ReLUs enablesefficient fully supervised training of deep networks. The ReLUs activations are more easily optimized than networks with sigmoid or tanh units.

VGG-19:

Create the model of VGG-19

Preprocessing the input

Extracting features

Flatten extracted features

Add Dense and dropout layers

Output

Results and Discussion

In this work, the ADNI dataset (1326 images) is used for evaluation. In this section, the Haralick features - ANN, LBP- ANN, Haralick-LBP ANN, and VGG-19 methods are evaluated using 10-fold cross validation. The algorithms are implemented using Python, open CV, tensor flow, and keras. The methods classify the input into 5 class - EMCI, LMCI, MCI, AD and CN. The accuracy, sensitivity, specificity and f measure as shown in tables 2 to 5and figures 5 to 8.

Table 2. Accuracy for VGG-19

	Haralick Features - ANN	LBP- ANN	Haralick-LBP ANN	VGG-19
Accuracy	82.74	84.11	86.69	91.05

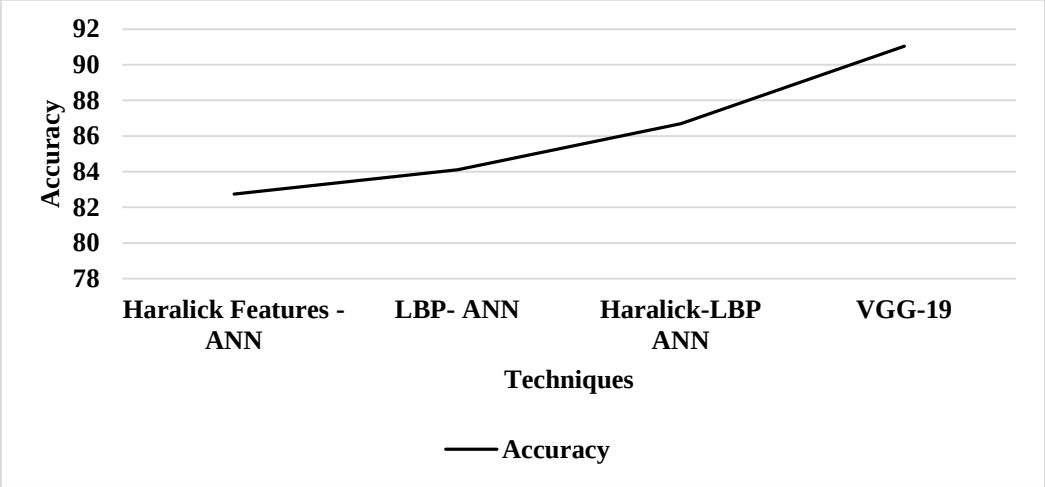

Figure 5. Accuracy for VGG-19

From the figure 5, it can be observed that the VGG-19 has higher classification accuracy by 9.56% for Haralick features - ANN, by 7.92% for LBP - ANN and by 4.91% for Haralick-LBP ANN respectively.

Table 3. Sensitivity for VGG-19

Sensitivity	Haralick Features - ANN	LBP- ANN	Haralick-LBP ANN	VGG-19
EMCI	0.8261	0.8435	0.8609	0.8957
MCI	0.8044	0.8178	0.8489	0.9022
LMCI	0.6571	0.7	0.7571	0.8
AD	0.7484	0.7742	0.8129	0.8968
CN	0.8804	0.8857	0.9054	0.9375

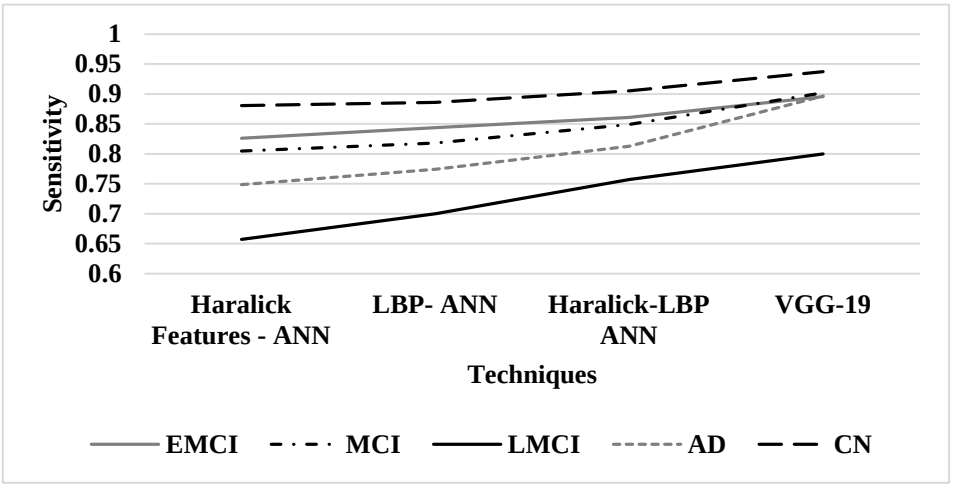

Figure 6. Sensitivity for VGG-19

From the figure 6, it can be observed that the VGG-19 has higher average sensitivity by 12.35% for Haralick features - ANN, by 9.72% for LBP - ANN and by 5.73% for Haralick-LBP ANN respectively.

Table 4. Specificity for VGG-19

Specificity	Haralick Features - ANN	LBP- ANN	Haralick-LBP ANN	VGG-19
EMCI	0.9543	0.9593	0.9669	0.9778
MCI	0.9473	0.9523	0.9588	0.9706
LMCI	0.9515	0.9549	0.9623	0.9781
AD	0.9489	0.9525	0.9615	0.9812
CN	0.9501	0.9563	0.9676	0.9695

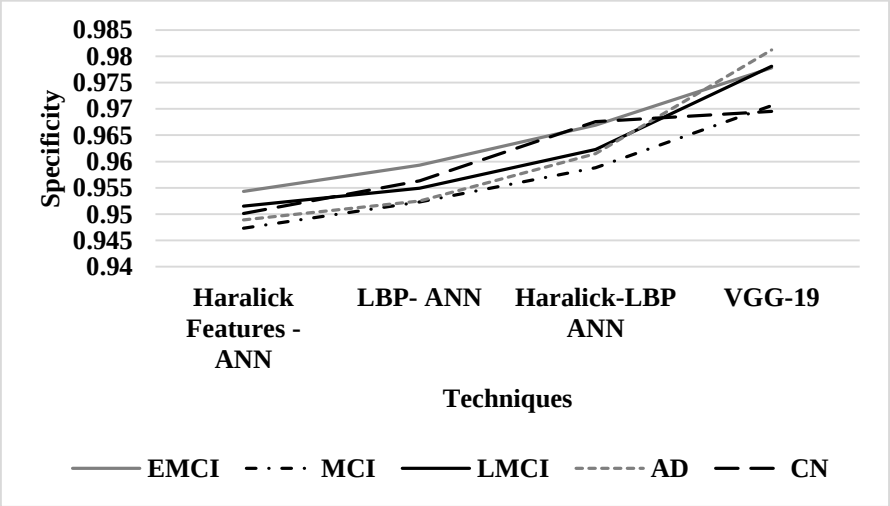

Figure 7. Specificity for VGG-19

From the figure 7, it can be observed that the VGG-19 has higher average specificity by 2.59% for Haralick features - ANN, by 2.11% for LBP - ANN and by 1.23% for Haralick-LBP ANN respectively.

Table 5. F Measure for VGG-19

F-Measure	Haralick Features - ANN	LBP- ANN	Haralick-LBP ANN	VGG-19
EMCI	0.8261	0.8435	0.8646	0.9016
MCI	0.7991	0.8142	0.8414	0.8903
LMCI	0.5542	0.5904	0.6503	0.7467
AD	0.725	0.7477	0.79	0.8882
CN	0.9122	0.9177	0.9337	0.9511

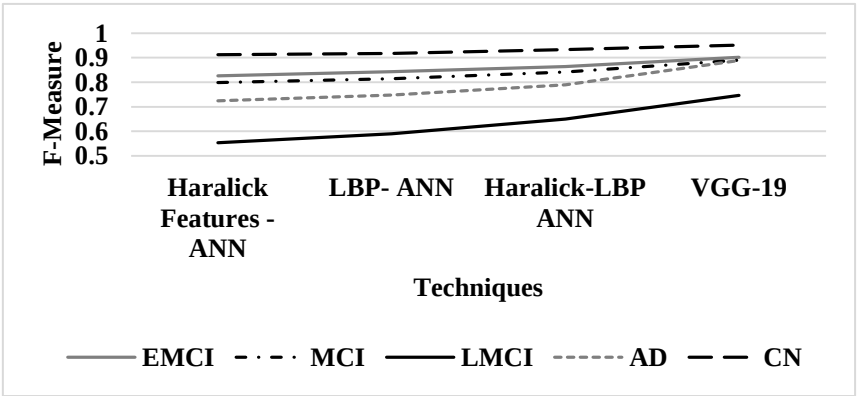

Figure 8. F Measures for VGG-19

From the figure 8, it can be observed that the VGG-19 has higher average f measure by 13.69% for Haralick features - ANN, by 11.2% for LBP - ANN and by 7.04% for Haralick-LBP ANN respectively.

The implementation screen shots are shown below figure 9 & 10.

Figure 9. Without Alzheimer's

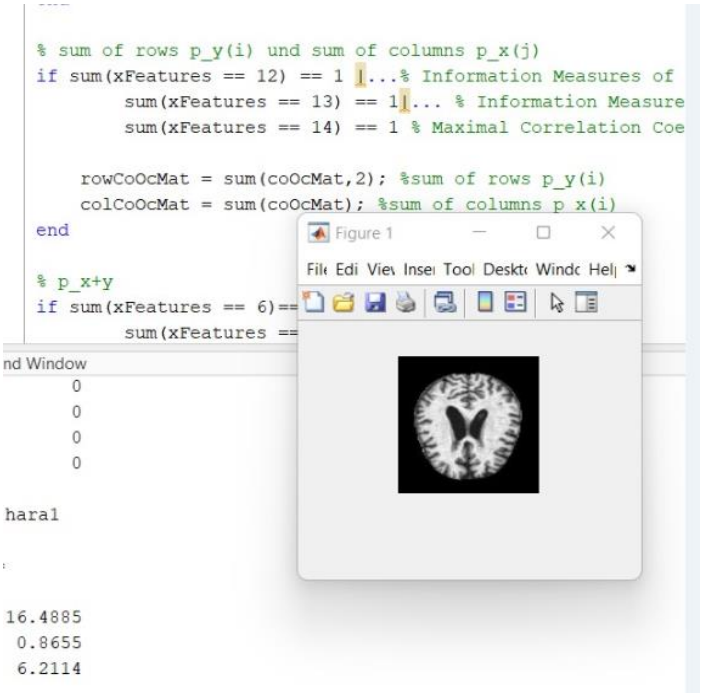

Figure 10. With Alzheimer's

Conclusion

Memory loss, behavioural problems, and poor self-care are all prominent symptoms of Alzheimer's disease (AD), one of the most prevalent neurodegenerative illnesses. A common prodromal MCI phase is marked by a gradual deterioration in memory. On the basis of the morphological as well as anatomical changes, the classification is done as EMCI, LMCI, MCI, AD and CN, in which MCI will represent an intermediate stage between AD and NC. Hence, clinical practices place a great importance on the AD's quantitative as well as qualitative diagnosis as it is able to offer additional period for the healing, and then enhance the patient's life quality as well as that of their caretakers. Unfortunately, diverse technical as well as clinical issues have resulted in limiting the power of the existing advanced diagnosis approaches in clinical practices. Furthermore, just a limited set of approaches have been exclusively intended for early AD forecast.

In this work, the Haralick and LBP techniques are used for feature extraction and deep learners for classification. This work has offered the proposal for a technologically advanced easy as well as early diagnosis scheme which will employ MRIs with the aid of advanced ML tools as well as algorithms like DL methods with VGG-19 network utilization. The VGG-19 was used to extract high-level DL features. The proposed methods were validated using 1240 images from ADNI dataset. Results show that the VGG-19 has higher classification accuracy by 9.56% for Haralick features - ANN, by 7.92% for LBP - ANN and by 4.91% for Haralick-LBP ANN respectively. Future work will investigate the optimization of hyper parameters of the CNN to improve the performance.

Conflict of interest

The authors declare no potential conflict of interest regarding the publication of this work. In addition, the ethical issues including plagiarism, informed consent, misconduct, data fabrication and, or falsification, double publication and, or submission, and redundancy have been completely witnessed by the authors.

Funding

The author(s) received no financial support for the research, authorship, and/or publication of this article

References

Aguilar, C., Westman, E., Muehlboeck, J. S., Mecocci, P., Vellas, B., Tsolaki, M., ... & Wahlund, L. O. (2013). Different multivariate techniques for automated classification of MRI data in Alzheimer's disease and mild cognitive impairment. Psychiatry Research: Neuroimaging, 212(2), 89-98.

Ahmed, S., Choi, K. Y., Lee, J. J., Kim, B. C., Kwon, G. R., Lee, K. H., & Jung, H. Y. (2019). Ensembles of patch-based classifiers for diagnosis of Alzheimer diseases. IEEE Access, 7, 73373-73383.

Altinkaya, E., Polat, K., & Barakli, B. (2020). Detection of alzheimer's disease and dementia states based on deep learning from MRI images: A comprehensive review. Journal of the Institute of Electronics and Computer, 1(1), 39-53.

Bevilacqua, V., Pietroleonardo, N., Triggiani, V., Brunetti, A., Di Palma, A. M., Rossini, M., & Gesualdo, L. (2017). An innovative neural network framework to classify blood vessels and tubules based on Haralick features evaluated in histological images of kidney biopsy. Neurocomputing, 228, 143-153.

Dhiman, G., Vinoth Kumar, V., Amandeep Kaur & Ashutosh Sharma., (2021), DON: Deep Learning and Optimization-Based Framework for Detection of Novel Coronavirus Disease Using X-ray Images. Interdiscip Sci Comput Life Sci 13, 260–272

Kale, V. V., Hamde, S. T., & Holambe, R. S. (2019). Brain disease diagnosis using local binary pattern and steerable pyramid. International Journal of Multimedia Information Retrieval, 8(3), 155-165.

Kang, S. K., Shin, S. A., Seo, S., Byun, M. S., Lee, D. Y., Kim, Y. K., ... & Lee, J. S. (2021). Deep learning-Based 3D inpainting of brain MR images. Scientific reports, 11(1), 1-11.

Kouser, R.R., Manikandan, T., Kumar, V.V (2018), "Heart disease prediction system using artificial neural network, radial basis function and case based reasoning" Journal of Computational and Theoretical Nanoscience, 15, pp. 2810-2817

Kumar, V. V., Raghunath, K. M. K., Rajesh, N., Venkatesan, M., Joseph, R. B., & Thillaiarasu, N. (2021). Paddy Plant Disease Recognition, Risk Analysis, and Classification Using Deep Convolution Neuro-Fuzzy Network. Journal of Mobile Multimedia. doi:10.13052/jmm1550-4646.1829

Lei, B., Liang, E., Yang, M., Yang, P., Zhou, F., Tan, E. L., ... & Wang, S. (2022). Predicting clinical scores for Alzheimer's disease based on joint and deep learning. Expert Systems with Applications, 187, 115966.

Liu, S., Masurkar, A., Rusinek, H., Chen, J., Zhang, B., Zhu, W., ... & Razavian, N. (2021). Development of a Deep Learning Model for Early Alzheime's Disease Detection from Structural MRIs and External Validation on an Independent Cohort. medRxiv.

Ljubic, B., Roychoudhury, S., Cao, X. H., Pavlovski, M., Obradovic, S., Nair, R., ... & Obradovic, Z. (2020). Influence of medical domain knowledge on deep learning for Alzheimer's disease prediction. Computer methods and programs in biomedicine, 197, 105765.

Lu, D., Popuri, K., Ding, G. W., Balachandar, R., Beg, M. F., & Alzheimer's Disease Neuroimaging Initiative. (2018). Multiscale deep neural network based analysis of FDG-PET images for the early diagnosis of Alzheimer's disease. Medical image analysis, 46, 26-34.

Mahesh, T. R., V. Dhilip Kumar, V. Vinoth Kumar, Junaid Asghar, Oana Geman, G. Arulkumaran, and N. Arun. (2022) "AdaBoost Ensemble Methods Using K-Fold Cross Validation for Survivability with the Early Detection of Heart Disease." Computational Intelligence and Neuroscience

Mohammed, B. A., Senan, E. M., Rassem, T. H., Makbol, N. M., Alanazi, A. A., Al-Mekhlafi, Z. G., ... & Ghaleb, F. A. (2021). Multi-Method Analysis of Medical Records and MRI Images for Early Diagnosis of Dementia and Alzheimer's Disease Based on Deep Learning and Hybrid Methods. Electronics, 10(22), 2860.

Muthukumaran V., Kumar, V. V., Joseph, R. B., Munirathanam, M., & Jeyakumar, B. (2021). Improving Network Security Based on Trust-Aware Routing Protocols Using Long Short-Term Memory-Queuing Segment-Routing Algorithms. International Journal of Information Technology Project Management, 12(4), 47–60. doi:10.4018/ijitpm.2021100105

Praveen Sundar, P.V., Ranjith, D., Vinoth Kumar, V, (2020). Low power area efficient adaptive FIR filter for hearing aids using distributed arithmetic architecture. Int J Speech Technol 23, 287–296. https://doi.org/10.1007/s10772-020-09686-y

Raghunath, K. M. Karthick, V. Vinoth Kumar, Muthukumaran Venkatesan, Krishna Kant Singh, T. R. Mahesh, and Akansha Singh (2022). "XGBoost Regression Classifier (XRC) Model for Cyber Attack Detection and Classification Using Inception V4." *Journal of Web Engineering*. doi:10.13052/jwe1540-9589.21413

Saba, S. S., Sreelakshmi, D., Kumar, P. S., Kumar, K. S., & Saba, S. R. (2020). Logistic regression machine learning algorithm on MRI brain image for fast and accurate diagnosis. International Journal of Scientific and Technology Research, 9(3), 7076-7081.

Taheri Gorji, H., & Kaabouch, N. (2019). A deep learning approach for diagnosis of mild cognitive impairment based on MRI images. Brain sciences, 9(9), 217.

Toğaçar, M., Cömert, Z., & Ergen, B. (2021). Enhancing of dataset using DeepDream, fuzzy color image enhancement and hypercolumn techniques to detection of the Alzheimer's disease stages by deep learning model. Neural Computing and Applications, 1-13.

V., Muthukumaran, Satheesh Kumar S., Rose Bindu Joseph, Vinoth Kumar V., and Akshay K. Uday (2021). "Intelligent Medical Data Analytics Using Classifiers and Clusters in Machine Learning." Advances in Computational Intelligence and Robotics : 321–335. doi:10.4018/978-1-7998-6870-5.ch022.

Bibliographic information of this paper for citing:

Allada A.; Bhavani, R.; Chaduvula, K. & Priya R. (2023). Early Diagnosis of Alzheimer Disease from Mri Using Deep Learning Models. *Journal of Information Technology Management,* 15 (Special Issue), 52-71. https://doi.org/ 10.22059/jitm.2022.89411